PORE-SCALE MICRO-CT IMAGING: CLUSTER SIZE DISTRIBUTION DURING DRAINAGE AND IMBIBITION

A. Georgiadis[1,2], S. Berg[1], G. Maitland[2], and H. Ott[1,*]
(1) Shell Global Solutions International BV, The Netherlands.
(2) Department of Chemical Engineering, Imperial College London, United Kingdom.

This paper was prepared for presentation at the International Symposium of the Society of Core Analysts held in Austin, Texas, USA 18-21 September, 2011

ABSTRACT
In the present study we investigate the size and volume distribution of *n*-decane clusters in a brine saturated porous glass sample by means of micro-CT imaging with pore-scale resolution. Cluster size distribution functions and cluster volumes were obtained by image analysis for a range of injected pore volumes under both imbibition and drainage conditions, and with a field of view larger than the porosity-based representative elementary volume (REV). *n*-decane clusters were found to be distributed in sizes greater than that of the REV, with the largest one containing between 65 and 99% of the entire non-wetting phase. The results indicate that the two-phase REV may be substantially larger than for single-phase flow and larger than the attainable field of view.

INTRODUCTION
In the geological sequestration of CO_2 in saline aquifers, a predominant question is how permanently the CO_2 is stored underground. The most immediate trapping mechanism is by capillary forces, i.e. formation of disconnected clusters of CO_2 (or in general of the non-wetting phase) in the porous medium. The storage permanency is dependent on the mobility of these clusters, which is closely linked to the cluster size and length on which a pressure gradient can act. Furthermore, the exact shape and size of these clusters define the rock/fluids and the fluid/fluid interfacial areas, which influence the kinetics of physical and chemical mass transfer between the different phases. This may further control the transition between different trapping mechanisms (from capillary trapping, to trapping by dissolution, and finally to mineralization). Micro computer tomography (μCT) enables direct pore space imaging at a resolution of few microns (μm) [1]. It has been demonstrated that fluid clusters can be imaged and the static cluster size distribution has been derived in some cases [2-6]. In these studies it has been shown that cluster size can range from a single pore to multiple-pore configurations. The cluster size distribution appears to peak at some typical value and then decay rapidly [2-5] or follow a power law in agreement with percolation theory [6].

In the present study we discuss the size distribution and volumes of non-wetting phase clusters in an *n*-decane/brine saturated porous glass sample during drainage and

imbibition. Porous glass was used as a model rock because of its well defined surface properties and of its suitable pore size for μCT imaging. *n*-decane was used as a proxy for the non-wetting phase, and the *n*-decane/brine interfacial tension (IFT) was varied by a surfactant in a range representative for CO_2/brine systems [7]. The fluid distribution in the porous medium was studied by means of μCT imaging with pore-scale resolution. The cluster sizes and volumes were extracted by image analysis for a range of injected pore volumes (PV) for both imbibition and drainage.

MATERIALS AND METHODS

n-decane (purity > 99 %) was used as non-wetting phase. The aqueous phase (wetting phase) was demineralized water with 4 wt-% CsCl (purity > 99 %) for enhancing the fluid/fluid CT contrast. The surfactant docecyl trimethyl ammonium bromide (DTAB, purity > 99 %) was introduced into the aqueous phase for selected experiments, at concentrations ranging both above and below the critical micelle concentration. The addition of surfactant was intended to lower the IFT to replicate the IFT for CO_2/brine systems under different thermodynamic conditions [7] without influencing other fluid properties like density and viscosity. The *n*-decane/DTAB-brine interfacial tension was measured with the du Noüy Ring method [7].

The experiments were carried out in a sintered glass core with a 10 mm diameter and a length of 20 mm. The porosity and permeability of the sample was experimentally determined to be $\phi = 0.318$ and $K = 20\text{-}24$ D, respectively. The core was embedded in a polycarbonate core holder by a shrinking process for a tight fit to avoid fluid bypassing. The flow geometry was vertical with fluid injection from top to bottom. The core holder was fixed onto the sample manipulation stage of the μCT scanner. The connection to the injection pumps and the production vessel was made by flexible PTFE tubing allowing a full 360^o rotation of the core, as is necessary for the tomography scans. The fluids were injected by means of two Quizix high precision displacement pumps, one for *n*-decane and the other for the brine phase. All wetted parts were thoroughly cleaned by sonication in isopropanol (purity > 99.5 %) for enabling well defined interfacial properties. The μCT scanner (ProCon X-Ray) was operated at 100 kV and 60 μA and at a resolution of 11.5 μm, which is a compromise between best spatial resolution, largest field of view and scanning time. The applicability of the resolution was verified against a high resolution scan (4.2 μm) by pore space analysis.

Before every experiment, the core was cleaned with at least 200 PV of isopropanol and was subsequently dried under vacuum. Prior to fluid injection, the sintered glass core was scanned in a dry state. Then an initial saturation with brine or *n*-decane was established by injection at 0.5 MPa pore pressure. All the following flooding experiments were performed at a constant flow rate of 1 ml/min, with a back pressure of 0.2 MPa. For the CT scans the injection was stopped and the inlet and outlet valves were closed. μCT scans at three different positions along the core were then conducted, each requiring approximately 20 min to complete. Following the completion of the scans for all three

positions, injection continued until a different PV value was obtained and CT scans were repeated. The raw images acquired were filtered by an FFT bandpass filter and then segmented by thresholding using *ImageJ*. The 3D pore space was derived from the segmented vacuum data sets and a porosity of 0.327 was calculated, which is in good agreement with the independently measured porosity of 0.318. This, together with the well reproduced permeability of 22 D as obtained from a single-phase Stokes flow simulation, validated the image filtering and thresholding applied. The *n*-decane saturation was derived from the segmented μCT data taken at the respective saturation states. Details are shown in Figs. 1 and 2.

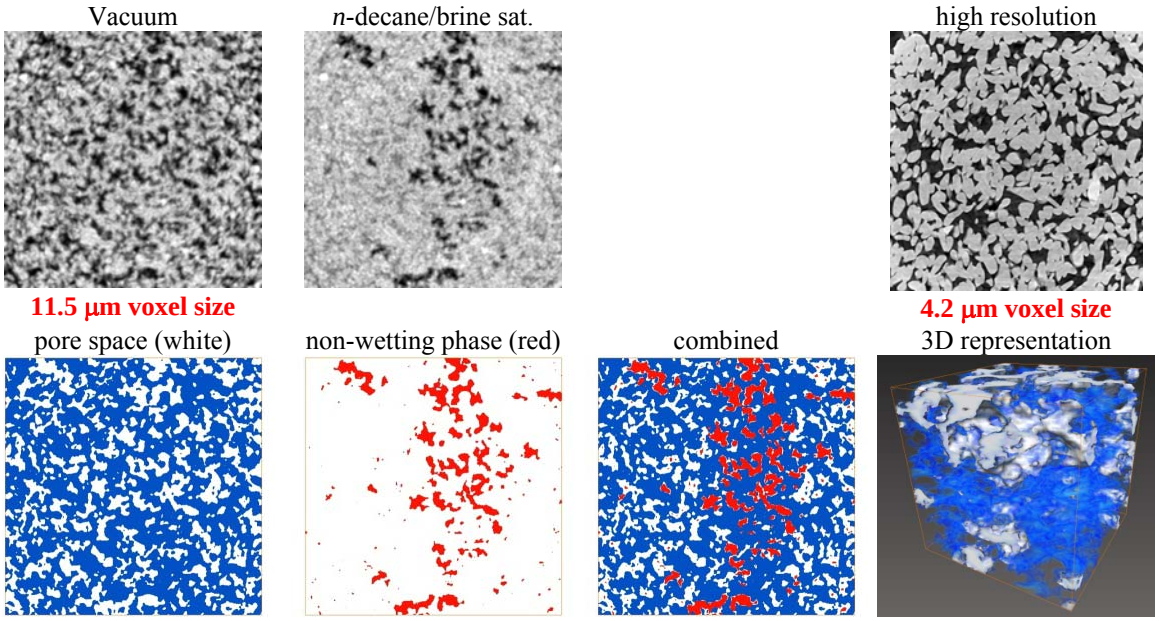

Figure 1: Upper row: μCT cross section in the dry state (low resolution on the left, high resolution on the right) and *n*-decane/brine saturated (middle). Lower row from left to right: pore space, non-wetting phase, and the superposition of both (2D). The far right image shows the 3D visualization (edge length 1.6 mm).

The upper row of Fig. 1 shows cross sections of raw data from the sample under vacuum (left), and after the injection of 1 PV of *n*-decane in the initially brine saturated sample (right). The CsCl concentration of the brine was chosen so that the contrast between glass grains and brine is minimized, achieving a clear contrast from the *n*-decane. Therefore, the *n*-decane volume could be directly derived by segmentation of the images of the saturated sample. The segmented images representing the total pore space and the non-wetting phase are shown in Fig. 1 below the respective raw data and are combined in 2D and 3D in the third and fourth images of the lower row, respectively.

RESULTS AND DISCUSSION

A sequence of flooding experiments were conducted by varying (a) the concentration of DTAB to adjust the IFT in a range corresponding to a capillary number of 10^{-5} and 10^{-4}

[8], respectively, and (b) the initial saturation and flooding sequence. For the experiments I (IFT=50.5 mN/m), IV (8.6 mN/m) and VI (27.2 mN/m), the core was pre-saturated with brine, and subsequently drained with 200 PV *n*-decane (drainage), before the imbibition was started. In experiments II (IFT=50.5 mN/m), III (8.6 mN/m) and V (27.2 mN/m) the sample was directly pre-saturated with *n*-decane and brine was injected thereafter. μCT scans were taken from the respective initial state and after injection of certain fluid volumes as indicated in the respective Figures (in PV). In Fig. 2, the 3D fluid saturation derived from the segmented data during drainage (sub volume) is shown. The brine saturated volume is displayed in blue and the *n*-decane saturation in white, showing the growth of the *n*-decane clusters as a function of the injected volume.

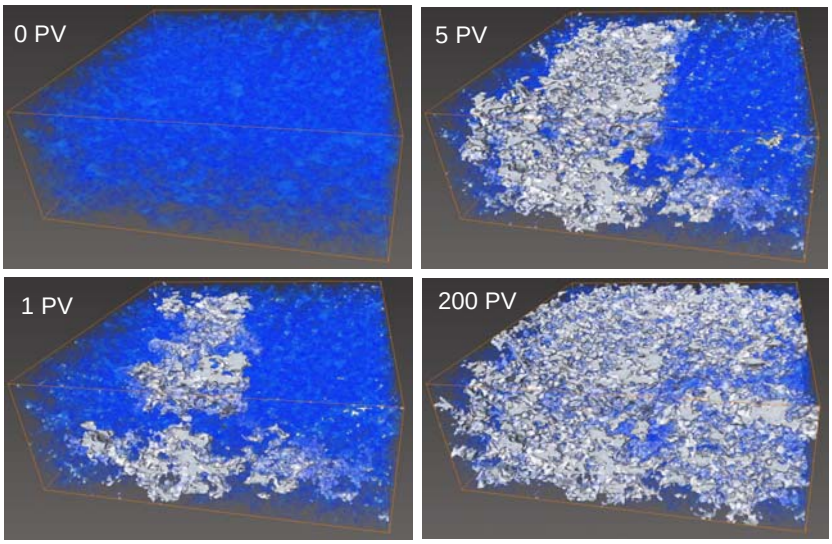

Figure 2: 3D fluid saturations during drainage. Clearly visible is the growth of the *n*-decane clusters (white). The base length of the sub volume is 7.4 mm.

In order to put the cluster lengths into perspective, the (single-phase, porosity based) representative elementary volume (REV) was determined from the porosity as a function of the averaging window, displayed on the left-hand side of Fig. 3. The field of view of the μCT scans is more than twice the REV in each direction. The pore size distribution (i.e. the pore radius distribution for the low and high resolution scan) was computed from the segmented vacuum scans [9]. The results are shown on the right-hand side of Fig. 3. The pore radius distribution assumes spherical pore geometry and peaks for both resolutions at approximately 30 μm, providing a measure for the pore size.

The segmented μCT data of the fluid saturated sample provides information about the distribution of the fluids in the porous space. Of particular interest is the size and the volume of the various trapped clusters. On the right-hand side of Fig. 3, the cluster length distribution is plotted, showing essentially two characteristic features: (1) the size distribution of the smaller clusters is very similar to that observed by Iglauer *et al.* [6], and (2), the *n*-decane clusters extend far beyond the largest pores and even the (porosity

based) REV. In Fig. 4 the volume of the largest cluster is plotted versus average *n*-decane saturation.

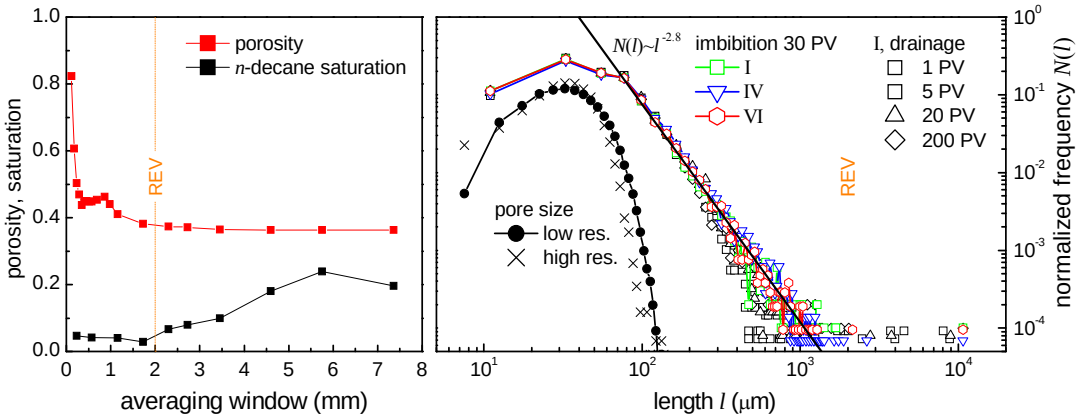

Figure 3: Left: porosity and saturation as a function of the averaging window. Right: Pore size distribution compared to the cluster size distribution of the non-wetting phase for different experimental runs.

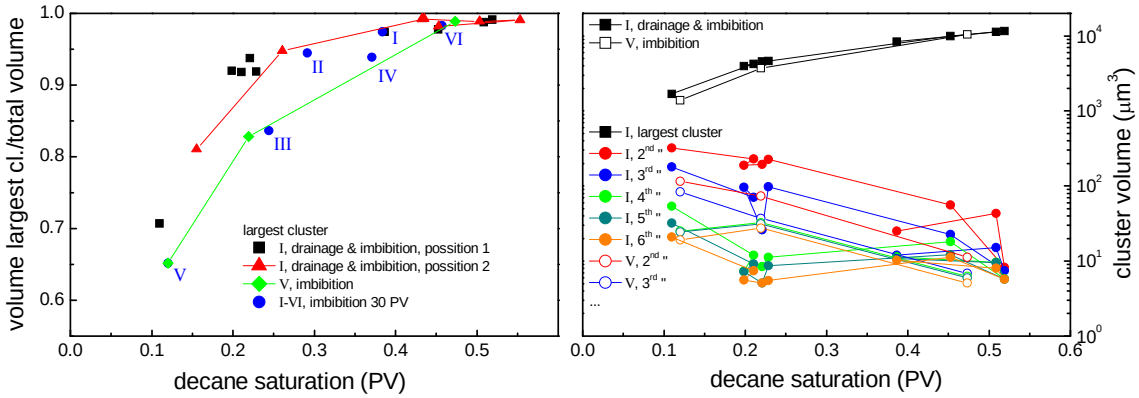

Figure 4: Left: Volume of the largest *n*-decane cluster over the total *n*-decane volume. Right: Length of the 6 largest clusters as function of brine saturation for different drainage and imbibition cycles. Large symbols and dotted line indicate imbibition experiments, small symbols and solid lines indicate drainage.

In Fig. 4 the volume of the largest cluster is plotted versus average *n*-decane saturation. The largest cluster contains 65 to 99% of the total *n*-decane volume. When the *n*-decane saturation is increased (drainage), the largest cluster grows at the expense of the smaller clusters, as is shown on the right hand side of Fig. 4. A similar behaviour but in the reverse direction is also observed for imbibition. When the *n*-decane saturation is decreased (imbibition), the largest cluster breaks apart and fragments into smaller clusters.

As illustrated in Fig. 4 there are only few large non-wetting phase clusters in the field of view, which raises the question of how representative this particular field of view was for the average saturation in the sample. Since we have established from the porosity that our field of view covered more than double the REV in each direction, we should be able to take 8 subsamples and find the same saturation value. It turned out that this depends

entirely on the sampling. For the saturation distribution shown in Fig. 2 for 5 PV of injected *n*-decane, for instance, when a sample cube with half length from the upper left corner at the front is selected, a high *n*-decane saturation is obtained. However, if the same volume is sampled from the upper right corner at the back, a very low *n*-decane saturation is found. This is also reflected in the saturation plotted as a function of the sampling volume added to the porosity plot on the left-hand side of Fig. 3. While the porosity becomes almost constant for averaging windows that are approximately half the field of view, the saturation still shows large variation. This means in practice that a two-phase REV can be much larger than a single-phase porosity based REV. The problem is essentially that the single largest cluster contains most of the non wetting phase and is likely to be not properly observed by the attainable field of view. This may be a property specific to this type of porous medium, which would have to be investigated in follow-up studies, i.e. how the cluster size depends for instance on the ratio of pore throat to pore body diameters.

CONCLUSION

Drainage and imbibition experiments in a sintered glass sample were performed and monitored by μCT scanning with pore scale resolution at different saturation steps. The representative elementary volume (porosity based REV), and the pore and cluster size distributions were analyzed. It was found that more than 65 to 99% of the non-wetting phase is contained in the largest cluster. When the average non-wetting phase saturation (drainage) is increased, the largest cluster grows at the expense of the next smaller clusters, and breaks apart again during imbibition. A potential two-phase REV has been found to be larger than the attainable field of view which can only be enlarged at the cost of resolution. But too low a resolution would make it increasingly impossible to determine the cluster connectivity.

REFERENCES

* Corresponding author; E-mail address: holger.ott@shell.com, research@holger-ott.de

1. See e.g.: Appoloni, C. R., Rodrigues, C. R. O., and Fernandes, C. P., *Proceedings of the International Symposium of the Society of Core Analysts*, Toronto, (2005) **SCA2005-41**.
2. Prodanović, M., Lindquist, W. P., and Seright, R. S., *Adv. Water Resour.* **30**, 214, (2007).
3. Kumar, M., Senden, T. J., Sheppard, A. P., Middleton, J. P., and Knackstedt, M. A., *Proceedings of the International Symposium of the Society of Core Analysts*, Noordwijk, (2009) **SCA2009-16**.
4. Kumar, M., Middleton, J. P., Sheppard, A. P., Senden, T. J., and Knackstedt M. A., *Proceedings of the International Petroleum Technology Conference*, Doha, (2009) **IPTC 14001**.
5. Karpyn, Z., Piri, M., and Singh G., *Water Resour. Res.* **46**, W04510 (2010).
6. Iglauer, S., Favretto, S., Spinelli, G., Schena, G., and Blunt, M. J., *Phys Rev E* **82**, 056315, (2010).
7. Georgiadis, A., Maitland, G., Trusler, J. P. M., and Bismarck A., *J Chem Eng Data*, (2010), **55**, 4168-4175.
8. The *n*-decane saturations obtained for different capillary numbers (*Ca*) were within the range in which the residual saturation starts to become a function of *Ca* (capillary de-saturation curve (L. W. Lake, 1989)). A trend of *n*-decane saturation as a function of IFT was observed, but the effect is in the order of the scatter induced by the relative positions of the larger clusters to the field of view.
9. The pore size distribution was computed with the Avizo XSkeleton, which is a skeletonization using an Euclidean distance map and thinning.